SIAM J. APPL. MATH.
Vol. 80, No. 3, pp. 1223–1246

TRANSIENT DYNAMICS OF A STOICHIOMETRIC CYANOBACTERIA MODEL VIA MULTIPLE-SCALE ANALYSIS*

CHRISTOPHER M. HEGGERUD†, HAO WANG†, AND MARK A. LEWIS‡

Abstract. Cyanobacterial (CB) blooms are becoming a global concern due to the increasing prevalence of eutrophication. The dependence of CB dynamics on phosphorus and light inputs is modeled via a stoichiometric approach. The dynamics occur in distinct phases that allow us to make use of multiple timescale analysis to uncover the driving mechanisms of each phase. As a result, we are able to approximate the length of time a bloom persists. This framework helps to establish the use of multiscale methods in stoichiometric models and provides deeper understanding of CB dynamics.

Key words. ecological stoichiometry, cyanobacteria, asymptotic analysis, multiscale analysis, harmful algal blooms, transient dynamics

AMS subject classifications. 92B05, 92D25, 92D40, 34E15, 34E13

DOI. 10.1137/19M1251217

1. Introduction.

Ecological systems are intricate and require key molecules and elements to function in an integrative nonlinear way. We can attempt to mechanistically model ecological systems in terms of these key molecules and elements. Ecological stoichiometry, the study of the balance of energy (such as light and carbon) and elemental resources (such as phosphorus and nitrogen) in ecological interactions and processes [32], is a powerful tool for studying and interpreting macroscopic phenomena via microscopic building blocks associated with nutrients and energy in an ecological system. Ecological stoichiometry has become increasingly popular in theoretical ecology [32, 11], and its predictions have been supported by an array of empirical studies [32, 6, 28, 2, 34]. While classical mathematical models cannot explain many observed ecological phenomena due to the lack of mechanistic modeling of limiting nutrients or energy, ecological stoichiometry allows us to mechanistically model the effects of limiting resources on ecological dynamics and trophic interactions [37, 1, 32, 2, 8, 22]. Some such models include producer-grazer interactions [36, 22], algae-bacteria interactions [37], organic matter decomposition [19], and toxin stress on various trophic interactions [13, 14, 29]. These studies show the crucial role that ecological stoichiometry has to play in the mechanistic modeling of biological dynamics and the successful interpretation of many existing paradoxes.

Harmful algal blooms (HABs) have become an issue of global concern in aquatic ecosystems [28]. HABs occur for a variety of reasons but most commonly are the result of eutrophication [27]. Eutrophication is described as an excess of nutrients required for organismal growth in a body of water. In North America, eutrophication is commonly caused by industrial, agricultural, and urban nutrient runoff [27]. In temperate regions these anthropogenic sources of nutrient promote the growth of algae

*Received by the editors March 22, 2019; accepted for publication (in revised form) February 19, 2020; published electronically May 19, 2020.
https://doi.org/10.1137/19M1251217
Funding: This work was supported by the NSERC, Alberta Innovates, Alberta Conservation Association, and a Canada Research Chair.

†Department of Mathematical and Statistical Sciences, University of Alberta, Edmonton, AB, Canada T6G 2G1 (cheggeru@ualberta.ca, hao8@ualberta.ca).
‡Department of Mathematical and Statistical Sciences and Department of Biological Sciences, University of Alberta, Edmonton, AB, Canada T6G 2G1 (mark.lewis@ualberta.ca).

and, perhaps more important, the growth of cyanobacteria (CB) [28]. Many genera of CB produce toxins, called cyanotoxins, which are harmful to humans, agriculture, and the aquatic dynamics within lakes and water bodies. A CB bloom can be detrimental to the aquatic ecosystem, causing toxification and anoxia. This results in low productivity of the ecosystem [28]. For these reasons it is important to understand how anthropogenic nutrient inputs and eutrophication influence HAB longevity and severity.

The majority of temperate lakes are stratified, meaning they are separated into two distinct thermal layers by a thermocline. The hypolimnion is the cold and stagnant layer, with little to no solar energy, which lies underneath the thermocline. Above the thermocline is the warmer, well-mixed, and more active layer called the epilimnion. Availability of sunlight in the epilimnion allows phytoplankton to grow provided there are sufficient nutrients available. Phosphorus is the most common limiting nutrient in temperate lakes, followed by nitrogen. Nutrients can be added to the water column through several distinct mechanisms, such as a slow mixing between stratified layers, inputs from rivers, rain or snowmelt runoff, and industrial or agricultural runoff [27]. Since phytoplankton growth depends on both light and available nutrients, we must also consider the stoichiometry of the phytoplankton when formulating models. Furthermore, the transient dynamics of the phytoplankton depend heavily on the initial nutrient concentration. Several models only consider the stratified water column when investigating phytoplankton dynamics [15, 24, 39]. Other models consider light limitation [23, 15]. Few have considered stratification, light limitation, and the stoichiometry of phytoplankton [37, 2].

Often, asymptotic dynamics, such as stability of equilibria or limit cycles, are the main focus of mathematical model analysis. However, the asymptotic dynamics can be misleading or uninformative when asking management questions pertaining to shorter timescales. For this reason transient dynamics, dynamics that occur on a smaller timescale, should not be overlooked [9]. A slight change in initial conditions or a perturbation can drastically alter the transient dynamics of an ecosystem. Understanding the transient dynamics and their sensitivity to changes may be crucial to management strategies aimed at short-term predictions of ecosystem behavior [9].

The dynamics of CB occur on multiple timescales. It is not uncommon for CB to persist at a low concentration of biomass for long periods. Once conditions are right, a fast increase in CB biomass occurs, often resulting in HABs. The blooms can persist for varied periods of time but often senesce quickly. Furthermore, CB have very small although varying nutrient-to-carbon ratios. Hence, the measures of internal nutrient and biomass are different orders of magnitude [38]. All of these factors inspire a multiple timescale analysis. Fortunately, the multiple timescale analysis allows us to study the driving mechanisms behind the transient dynamics of CB.

Singular perturbation theory boasts a broad range of biological applications. This theory is based on the limiting behavior of multiscale dynamics, a common biological feature. The theory from singular perturbations used for multiple timescales typically employs asymptotic techniques, such as matching and series expansions [20]. Perhaps most relevant to our study is the theory developed by Neil Fenichel that gives a geometric interpretation of phase spaces of perturbed systems with relation to the simpler unperturbed system [7]. This theory allows applied mathematicians to perform analysis on simplified versions of complex systems and draw conclusions about the complex system. Furthermore, this theory allows the in-depth study of the transient dynamics of a system, which is of great importance to ecosystem management and ecological predictions [9]. Singular perturbation theory is by no means

new and has been utilized in several milestone models in biology, such as the Van der Pol oscillator [35, 3], the Hodgkin–Huxley model [12, 31], Michaelis–Menton enzyme kinetics [17], and, more recently, predator-prey dynamics [30, 10] as well as in numerous applications outside biology. *To our best knowledge, no rigorous application of the theory has yet been applied to stoichiometric models in ecology. In this paper we provide a rigorous application of multiscale methods to understand the transient dynamics of a stoichiometric CB model.* The mathematical analysis also yields an interesting type of dynamics at the fold curve [10, 20]. That is, the transient dynamics transition from one slow submanifold to another, as discussed in section 5.

We extend the stoichiometric model of Wang et al. [37] to consider the dynamics under various initial levels of dissolved mineral phosphorus. The various levels of dissolved mineral phosphorous are representative of the level of eutrophication. We notice from the numerical simulation, shown in section 3, that interesting transient dynamics arise, inspiring a multiple timescale analysis. In section 4 we perform the multiple timescale analysis and mathematically describe the dynamics presented in section 3. In section 4 we show that, for certain initial conditions, a "switch" in the dynamics from being light limited to phosphorus limited must occur. In section 6 we approximate the longevity of blooms with regard to the initial eutrophication level, initial conditions, and model parameters. Finally, we discuss how these results create a deeper biological understanding of transient CB dynamics and discuss the mathematical implications in section 7. The results presented in this paper show the unique application of multiscale methods to stoichiometric models and how useful they can be in applying the results to real-world systems.

2. Model formulation. In this section we discuss the biological background, mechanisms, and assumptions used to construct our model. The model consists of three interconnected variables, B, Q, and P, that represent the concentration of carbon biomass of CB, phosphorus cell quota, and concentration of mineral phosphorus, respectively. To track the rates of change of each variable, we use a system of three interconnected nonlinear differential equations. The derivation of the model follows that of Berger et al. [2] and Wang et al. [37].

We assume the dynamics occur in a well-mixed epilimnion with depth z_m. We assume that water exchange with respect to the epilimnion occurs via two mechanisms. First, we assume that water is exchanged between the epilimnion and the hypolimnion. Second, we assume that water is exchanged between the epilimnion and the inflow/outflow of rivers, rain runoff, and springs. We assume that both water exchange mechanisms occur at rate D. Furthermore, we assume that the concentration of phosphorus is constant and equal in both the hypolimnion and the inflow, denoted with p_{in}. The rate of concentration change of CB and phosphorus due to the water exchange is proportional to the volume of the epilimnion. That is, the amount of particulates exchanged is related to the proportion of particulates located near the boundaries. In a larger volume, a smaller proportion of total substrate lies near the epilimnion boundaries. On the other hand, in a smaller volume, a larger proportion of substrates in the epilimnion will be exchanged. Hence, the particulate exchange rate, in and out, is inversely proportional to the depth of the well-mixed epilimnion.

CB lose carbon through respiration, resulting in a decrease of carbon biomass [38]. Assuming sufficient nutrients, CB photosynthesis and thereby growth depend on light availability throughout the epilimnion. The light intensity along the water column is attenuated by cyanobacteria and other suspended particles. Following the Lambert–Beer law [15], we model the light intensity at a given water depth, s, and

TABLE 1
Definitions and values for parameters of system (2.4).

Parameter	Meaning	Value for simulation	Biological values	Reference
r	Maximum CB-specific production rate	1	1/day	[4]
Q_m	CB cell quota at which growth ceases (minimum)	0.004	0.004 gP/gC	[4]
Q_M	CB cell quota at which nutrient uptake ceases (maximum)	0.04	0.04 gP/gC	[4]
z_m	Depth of epilimnion	7	$>0-10$m	[16]
ν_r	CB respiration loss rate	0.35	$0.05-0.6$/day	[38, 2]
D	Water exchange rate	0.02	m/day	[2]
H	Half-saturation coefficient of light-dependent CB production	120	120 μ mol/(m$^2\cdot$ s)	[4]
ρ_m	Maximum CB phosphorus uptake rate	1	0.2–1 gP/gC/day	[2, 4]
M	Half-saturation coefficient for CB nutrient uptake	1.5	1.5 mgP/m^3	[4]
P_{in}				
p_{in}	Concentration of dissolved inorganic phosphorus in the hypolimnion and inflow	5	$0-150$ mgP/m^3	[2]
K_{bg}	Background light attenuation	0.3	$0.3-0.9$/m	[2, 4]
k	Algal-specific light attenuation	0.0004	$0.0003-0.0004$ m^2/mg C	[2, 4]
I_{in}	Light intensity at water surface	300	300 μ mol/(m$^2\cdot$ s)	[4]

CB biomass concentration, B, by

$$L(s,B) = I_{in}\exp\left[-(K_{bg}+kB)s\right]. \tag{2.1}$$

The parameters I_{in}, K_{bg}, and k_b are described in Table 1. The light-dependent CB growth is modeled with the Monod equation, $\frac{L(s,B)}{L(s,B)+H}$, which is empirically supported [18]. However, this function is depth dependent. Thus, applying the well-mixed assumption, we average the carbon/energy production function over the depth of the epilimnion. The light-dependent CB growth function is

$$h(B) \equiv \frac{1}{z_m}\int_0^{z_m} \frac{L(s,B)}{L(s,B)+H}ds. \tag{2.2}$$

This integral is easily evaluated and used in later analysis. The internal phosphorus-dependent growth function follows the empirically well-tested Droop form, $1-\frac{Q_m}{Q}$, where Q_m is the minimum cell quota. The product of the light and phosphorus-dependent CB growth functions scales the maximum CB reproduction rate, r, as $rB(1-\frac{Q_m}{Q})h(B)$.

Nutrient uptake is a decreasing function of CB cell quota. Uptake is maximal when the cell quota is at its minimum, Q_m, but should cease when the cell quota is at its maximum, Q_M. Nutrient uptake follows the empirically supported Monod form [26], which is a saturating function of dissolved mineral phosphorous. These assumptions yield the nutrient uptake function

$$\rho(Q,P) = \rho_m\Big(\frac{Q_M-Q}{Q_M-Q_m}\Big)\frac{P}{P+M}, \tag{2.3}$$

where ρ_m and M are the maximum phosphorus uptake rate and the half-saturation coefficient for CB phosphorus uptake, respectively.

The combination of the above assumptions yields the following stoichiometric CB model:

$$\begin{cases} \dfrac{dB}{dt} = \underbrace{rB\Big(1-\dfrac{Q_m}{Q}\Big)h(B)}_{\text{growth limited by P and light}} - \underbrace{\nu_r B}_{\text{respiration}} - \underbrace{\dfrac{D}{z_m}B}_{\text{exchange}}, \\ \dfrac{dQ}{dt} = \underbrace{\rho(Q,P)}_{\text{replenishment}} - \underbrace{rQ\Big(1-\dfrac{Q_m}{Q}\Big)h(B)}_{\text{cell quota dilution due to cell division}}, \\ \dfrac{dP}{dt} = \underbrace{\dfrac{D}{z_m}(p_{in}-P)}_{\text{P input and exchange}} - \underbrace{B\rho(P,Q)}_{\text{P consumption}}. \end{cases} \tag{2.4}$$

We also denote the total phosphorus concentration in the system by $R = BQ + P$. All parameter definitions and values used throughout this paper are found in Table 1. The parameter values listed are representative of realistic phytoplankton traits. Global qualitative analysis and bifurcation plots of model (2.4) were discussed by Wang et al. [37] and will not be restated here. For the purpose of this paper, we are interested in the transient dynamics for various initial conditions. In particular, we study how the dynamics depend on the initial phosphorus concentration, as it is a descriptor of how eutrophic the environment is initially.

3. Model simulation. In this section we simulate model (2.4) for one year to illustrate the unique qualitative nature of the dynamics. To motivate the analysis of future sections, we notice abrupt transition layers in B and Q, as seen in Figure 1, that are now understood to be triggered by a slow change in phosphorus concentration. We seek to compute the times at which the abrupt transitions will occur. This provides important insight into understanding bloom longevity. One could easily compute this time duration numerically, but we show in section 6 that we can approximate the longevity of the bloom as a function of model parameters and initial conditions.

Figure 1 illustrates the model dynamics simulated over one year. The dynamics can be described as four separate phases. First is the sudden growth, or onset, of the CB bloom. This phase is encouraged by rapid uptake of phosphorus, as we discuss in section 4.2, allowing the CB to grow at a rate near its maximum. Second is the extended period of time where the bloom is not growing but remains at a high level. Here, the CB phosphorus uptake is constant, resulting in a slow decrease in available phosphorus. Also, the CB reach a biomass level where self-shading occurs, causing their growth to be light limited [38]. The third phase involves the abrupt decrease in both cell quota and CB. In this phase, the phosphorus concentration has become essentially depleted. This results in the fourth phase, where all variables tend to a low equilibrium. We discuss each phase in greater detail in the following sections.

4. Multiple timescale dynamics. In this section we explain mathematically the mechanisms responsible for the phases and for the transitions between them discussed in section 3. We begin with a nondimensionalization of model (2.4) given by (4.1) and determine that the system contains small perturbation parameters. We proceed by deriving fast and slow subsystems of (4.1). The fast subsystem explains the abrupt uptake of phosphorus. The slow subsystem allows us to understand the

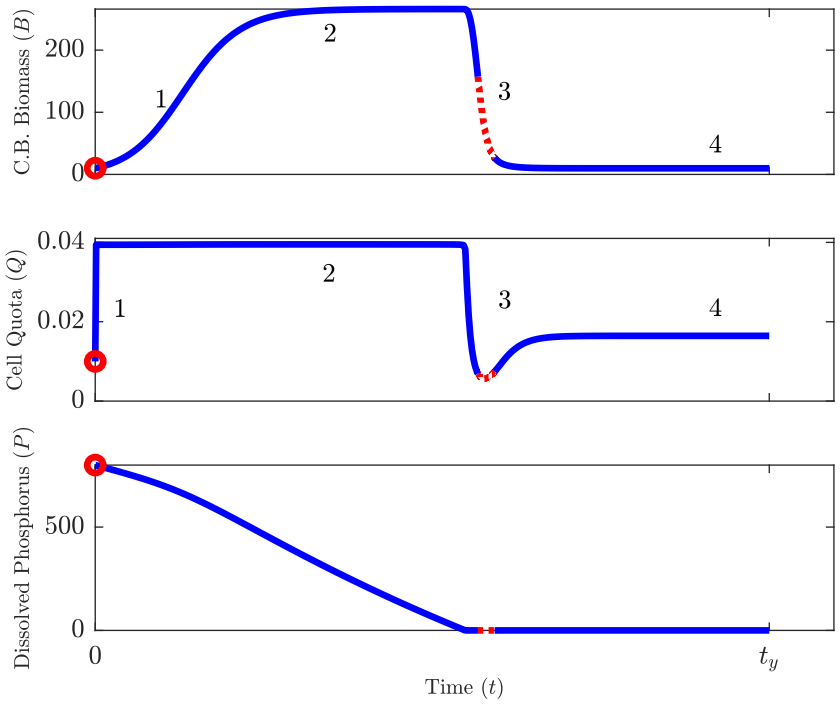

FIG. 1. *Dynamics of model* (2.4) *with parameter values listed in Table* 1. *The dynamics involve four main phases;* (1) *the abrupt increase of cell quota and CB biomass,* (2) *the apparent bloom phase,* (3) *the sudden crash of the cell quota and CB biomass, and* (4) *the low constant phase.* $t_y = 365$ *days, and the solid blue portions of the curves represent when light is limiting growth. The red dotted portions represent when phosphorous is limiting.*

transition layers by looking at the unique characteristics of the critical manifold. This analysis finally allows us to approximate the longevity of the bloom.

4.1. Nondimensionalization. We rescale system (2.4) to achieve dimensionless variables and parameters. The dimensionless system is given below:

$$\frac{du}{d\tau} = u\Big(1 - \frac{1}{\gamma v}\Big)\frac{1}{u + k_1}\log\Big(\frac{1+I}{1 + I\exp(-u - k_1)}\Big) - (\alpha + \beta)u = ug(u, v; \beta), \tag{4.1a}$$

$$\delta\frac{dv}{d\tau} = (1 - v)\frac{w - \sigma uv}{w - \sigma uv + \mu} + \delta\Big(\frac{1}{\gamma} - v\Big)\frac{1}{u + k_1}\log\Big(\frac{1+I}{1 + I\exp(-u - k_1)}\Big) = f(u, v, w; \delta), \tag{4.1b}$$

$$\frac{dw}{d\tau} = -\alpha\sigma uv - \beta(w - 1) = h(u, v, w; \beta), \tag{4.1c}$$

with $u = kz_mB$, $v = \frac{Q}{Q_M}$, $w = \frac{R}{p_{in}} = \frac{P+BQ}{p_{in}}$, and $\tau = rt$. The parameters and their respective dimensionless quantities are given in Table 2.

This scaling allows all state variables to be of order one. However, β and δ are smaller than other parameters and will be treated as small independent perturbation parameters each of which is biologically motivated. The parameter β is directly

TABLE 2
Dimensionless parameters for system (4.1).

Parameter	Definition	Value
α	ν_r/r	0.35
β	$\dfrac{D}{rz_m}$	0.0029
δ	$\dfrac{r(Q_M - Q_m)}{\rho_m}$	0.036
μ	M/p_{in}	0.3
γ	$\frac{Q_M}{Q_m}$	10
σ	$\dfrac{Q_M}{p_{in}z_m k}$	2.9
k_1	$z_m K_{bg}$	2.1
I	I_{in}/H	2.5

proportional to the exchange rate between the hypolimnion, or inflows and outflows, and the epilimnion. In stagnant or deep stratified lakes, β is small. The parameter δ is proportional to $Q_M - Q_m$, the difference between maximum and minimum cell quota. The cell quotas are considered small, as the phosphorus-to-carbon ratio of a single cell is naturally small, even at the maximum [4, 38]. Note that when $\beta = 0$, the structure of the system is qualitatively the same as when β is nonzero; thus, β acts as a regular perturbation. When $\delta = 0$, the system is reduced to an algebraic-differential system; for this reason, we say δ causes a singular perturbation.

4.2. Fast timescale dynamics. In this section we study the fast system. We show that the abrupt uptake of phosphorus that motivates the bloom occurs on the fast timescale and use this to understand the first phase of the dynamics shown in Figure 1. Furthermore, we obtain the first-order approximation of the system on the fast timescale, which will then be used to form the uniform first-order approximation.

We introduce the intermediate variable $\xi(\beta, \delta)$ so that the fast timescale is $t_1 = \tau/\xi(\beta, \delta)$, where ξ is to be determined. Let $U(t_1) = u(\xi t_1)$, $V(t_1) = v(\xi t_1)$, and $W(t_1) = w(\xi t_1)$. Then U, V, and W are functions of the fast time variable and are referred to as the fast variables. The fast system dynamics are then given by the following system of equations:

$$
\begin{aligned}
\frac{1}{\xi(\beta,\delta)}\frac{dU}{dt_1} &= U\Big(1 - \frac{1}{\gamma V}\Big)\frac{1}{U + k_1}\log\Big(\frac{1+I}{1 + I\exp(-U - k_1)}\Big) - (\alpha + \beta)U,\\
\frac{1}{\xi(\beta,\delta)}\delta\frac{dV}{dt_1} &= (1 - V)\frac{W - \sigma UV}{W - \sigma UV + \mu}\\
&\qquad + \delta(1/\gamma - V)\frac{1}{U + k_1}\log\Big(\frac{1+I}{1 + I\exp(-U - k_1)}\Big),\\
\frac{1}{\xi(\beta,\delta)}\frac{dW}{dt_1} &= -\alpha\sigma UV - \beta(W - 1).
\end{aligned}
\tag{4.2}
$$

We choose $\xi(\beta, \delta) = \delta$ in order to retain the term involving $\frac{dV}{dt}$. After applying the two-parameter asymptotic expansion in β and δ (see Appendix A) for each of the fast

variables and letting $\beta, \delta \to 0$, we obtain the subsystem that describes the first-order approximation of the fast time variables:

$$\begin{aligned} \frac{dU_{0,0}}{dt_1} &= 0, \\ \frac{dV_{0,0}}{dt_1} &= (1 - V_{0,0}) \frac{W_{0,0} - \sigma U_{0,0} V_{0,0}}{W_{0,0} - \sigma U_{0,0} V_{0,0} + \mu}, \\ \frac{dW_{0,0}}{dt_1} &= 0. \end{aligned} \tag{4.3}$$

We let $U_{00}(t_1) = u(0)$ and $W_{00}(t_1) = w(0)$ in order to satisfy the initial conditions. There are two possible equilibrium values, $V_{0,0} = 1$ and $V_{0,0} = W_{00}/\sigma U_{00}$. Note that

$$w(\tau) - \sigma u(\tau) v(\tau) \geq 0 \tag{4.4}$$

and

$$1/\gamma \leq v(\tau) \leq 1 \tag{4.5}$$

are biological restrictions representing the dissolved mineral phosphorus and the cell quota restrictions, respectively. Of course, these biological restrictions apply to the fast variables as well. Thus, depending on the initial conditions, at least one of the equilibria is biologically unfeasible.

Since U_{00} and W_{00} are constant, the differential equation for V_{00} in (4.3) is separable and easily solved. The implicit solution is given by

$$\frac{b-1}{1-a} \log(1 - V) - \frac{a-b}{1-a} \log(a - V) = t + C, \tag{4.6}$$

where $a = \frac{W}{\sigma U}$, $b = \frac{\mu}{\sigma U} + a$, and C is determined by the initial conditions. Note that the biological restrictions on the initial conditions and flow ensure that $(1-V), (a-V) \geq 0$. The solution to the fast system can only be given implicitly; however, we are still able to determine several more characteristics of the solution.

If we assume that $a > 1$, then as $t \to \infty$, the left-hand side of (4.6) tends to ∞. Since $V(0) < 1$ and $\frac{dV}{dt_1}$ is positive, it is clear that $V(t_1)$ is monotone increasing with a horizontal asymptote $V = 1$.

We now assume that $a < 1$. Then as $t \to \infty$, the left-hand side of (4.6) tends to ∞. Since $V(0) < a$ and $\frac{dV}{dt_1}$ is positive, it is clear that $V(t_1)$ is monotone increasing with a horizontal asymptote $V = a$.

We now conclude that

$$\lim_{t_1 \to \infty} V_{00} = \min\{1, a\} = \min\left\{1, \frac{w(0)}{\sigma u(0)}\right\}, \tag{4.7}$$

which satisfies the biological restriction (4.4).

To determine concavity, we compute

$$\frac{d^2V}{dt^2} = -\frac{dV}{dt}(b - V)^{-2}[V^2 - 2bV + ab + b - a]. \tag{4.8}$$

By Descartes' rule of sign, the quadratic term has either two or zero positive roots. Hence, $\frac{d^2V}{dt^2}$ can change signs either twice or never; this number depends on the discriminant $4b^2 - 4(ab + b - a)$. The zeros occur at

$$V = b \pm \sqrt{b^2 - ab - b + a} \tag{4.9}$$

$$= b \pm \sqrt{(b-a)(b-1)} \tag{4.10}$$

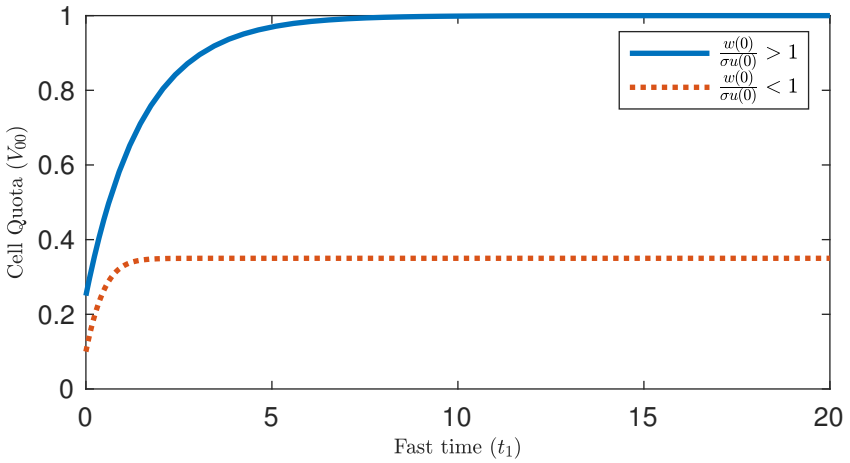

FIG. 2. *First-order approximation of cell quota (V_{00}) dynamics on the fast timescale for two different sets of initial conditions with parameter values given in Table 2. The dotted curve shows the dynamics for $\frac{w(0)}{\sigma u(0)} < 1$ and the solid curve for $\frac{w(0)}{\sigma u(0)} > 1$. On the fast timescale, the CB biomass (U_{00}) and total phosphorus (W_{00}) remain constant at their initial values.*

and at equilibria. Thus, if $b < 1$, then there are no real roots. Furthermore, if $b \geq 1$, then two positive roots appear. However, it is easily verified that $b \pm \sqrt{(b-a)(b-1)} > \min\{1, a\}$, and recalling that $1/\gamma \leq V \leq \min\{1, a\}$, we conclude that there are no inflection points in the domain. Furthermore, it is easy to see that $\frac{d^2V}{dt^2} < 0$ for $1/\gamma < V < \min\{1, a\}$. Hence, $V(t)$ is concave down in its domain. The dynamics of V_{00} for each case are shown in Figure 2.

4.3. Slow timescale dynamics. In this section we study the slow system. We show that the growth of CB is motivated by its fast P uptake and is dependent on the available P to sustain its growth. We show that once the P concentration becomes too low, the bloom can no longer be sustained. This is mathematically described as a transition from one submanifold of the critical manifold to another. Furthermore, we obtain the first-order approximation of the system on the slow timescale and will later use this to obtain a uniform first-order approximation.

We assume that the slow timescale is given by $t_2 = \tau$. Again, applying the asymptotic expansion (see Appendix A) to the slow variables and letting $\beta, \delta \to 0$, we arrive at the following slow system:

$$\begin{aligned} \frac{du_{00}}{dt_2} &= u_{00}\Big(1 - \frac{1}{\gamma v_{00}}\Big)\frac{1}{u_{00} + k_1} \log\Big(\frac{1+I}{1 + I\exp(-u_{00} - k_1)}\Big) - \alpha u_{00} \\ 0 &= (1 - v_{00})\frac{w_{00} - \sigma u_{00} v_{00}}{w_{00} - \sigma u_{00} v_{00} + \mu}, \\ \frac{dw_{00}}{dt_2} &= -\alpha\sigma u_{00} v_{00}. \end{aligned} \tag{4.11}$$

The slow system becomes an algebraic-differential system constrained by the set satisfying

$$0 = (1 - v_{00})\frac{w_{00} - \sigma u_{00} v_{00}}{w_{00} - \sigma u_{00} v_{00} + \mu}. \tag{4.12}$$

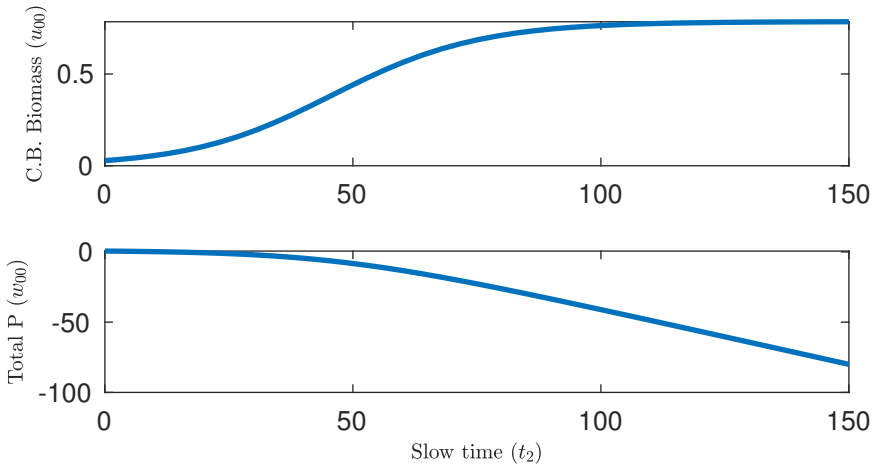

FIG. 3. *Slow scale dynamics of* (4.15) *with parameter values given in Table* 2 *and initial conditions such that* $w_{00}/\sigma u_{00} > 1$. *In this case,* $v_{00} = 1$, *and the dynamics occur on* M_0^0.

The critical manifold, M_0, is a subset of the set given by (4.12). The set (4.12) can be divided into two submanifolds. Furthermore, the variables are only defined within the biological domain $\mathcal{D} = \{(u, v, w) | w - \sigma uv \geq 0, \frac{1}{\gamma} \leq v \leq 1, u, w \geq 0\}$. Thus, relevant manifolds and submanifolds are within $\mathcal{D}$. We define the submanifolds as

$$M_0^0 = \{(u, v, w) : v_{00} = 1\} \cap \mathcal{D}, \tag{4.13}$$

$$M_0^1 = \{(u, v, w) : w_{00} - \sigma u_{00} v_{00} = 0\} \cap \mathcal{D}. \tag{4.14}$$

Furthermore, let $\mathcal{C} = M_0^0 \cap M_0^1 = \{(u, v, w) : w = \sigma u, v = 1\}$. Note that $M_0^0 \cup M_0^1 = \{(u, v, w) : 0 = (1 - v_{00}) \frac{w_{00} - \sigma u_{00} v_{00}}{w_{00} - \sigma u_{00} v_{00} + \mu}\} \cap \mathcal{D}$. Also, on M_0^0, the restriction (4.4) is equivalent to $\frac{w_{00}}{\sigma u_{00}} \geq 1$. We initially study the dynamics on each submanifold separately.

4.3.1. Dynamics on M_0^0. Here, we examine the dynamics of system (4.11) restricted to the submanifold M_0^0. On M_0^0, $v_{00} = 1$, and we write system (4.11) as

$$\begin{aligned} \frac{du_{00}}{dt_2} &= u_{00}\Big(1 - \frac{1}{\gamma}\Big) \frac{1}{u_{00} + k_1} \log\Big(\frac{1 + I}{1 + I \exp(-u_{00} - k_1)}\Big) - \alpha u_{00}, \\ \frac{dw_{00}}{dt_2} &= -\alpha \sigma u_{00}. \end{aligned} \tag{4.15}$$

The trivial equilibrium, $u_{00} = 0$, is unstable when $(1 - \frac{1}{\gamma}) \frac{1}{k_1} \log \frac{1+I}{1+I \exp(-k_1)} > \alpha$, which is true for the parameter values considered. That is, u_{00} will remain positive for all time, forcing w_{00} to diverge to negative infinity. Figure 3 shows the dynamics of this case for appropriate initial conditions. For appropriate initial conditions, these dynamics will eventually violate the biological restriction (4.4). However, we show in later sections how this violation is avoided by allowing the dynamics to switch to the submanifold M_0^1.

4.3.2. Dynamics on M_0^1. Here, we examine the dynamics of system (4.11) restricted to the submanifold M_0^1. On M_0^1, $w_{00} = \sigma u_{00} v_{00}$, and we write system

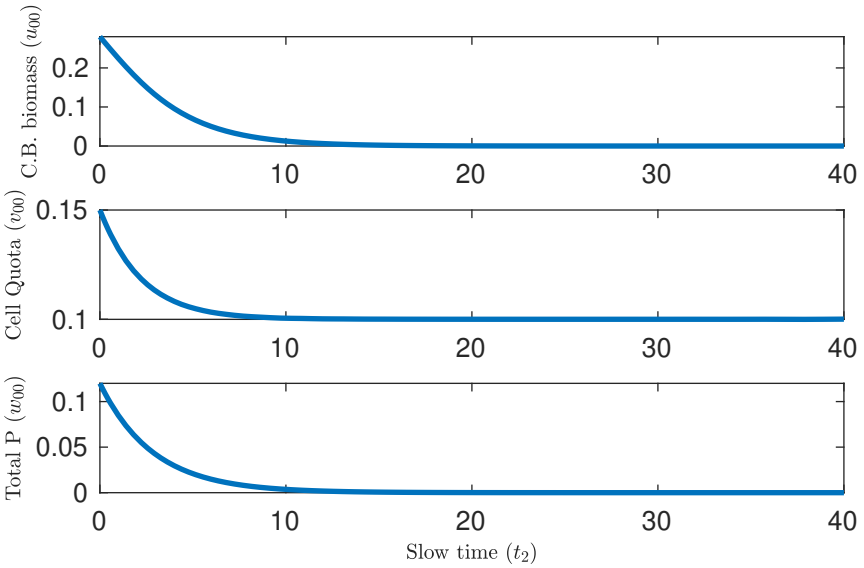

FIG. 4. *Slow scale dynamics given by system* (4.16) *with parameter values given by Table* 2 *and initial conditions such that* $w_{00}/\sigma u_{00} < 1$. *Here,* $v_{00} = w_{00}/\sigma u_{00}$, *and the dynamics occur on* M_0^1.

(4.11) as

$$\begin{aligned} \frac{du_{00}}{dt_2} &= u_{00}\Big(1 - \frac{1}{\gamma w_{00}/\sigma u_{00}}\Big)\frac{1}{u_{00}+k_1}\log\Big(\frac{1+I}{1+I\exp(-u_{00}-k_1)}\Big) - \alpha u_{00}, \\ \frac{dw_{00}}{dt_2} &= -\alpha w_{00}. \end{aligned} \tag{4.16}$$

In this case, w_{00} will decay to zero. The term $(1 - \frac{1}{\gamma w_{00}/\sigma u_{00}})$ is always positive; however, as w_{00} decays, $(1 - \frac{1}{\gamma w_{00}/\sigma u_{00}})$ will become increasingly small. Eventually, $-\alpha u_{00}$ will dominate, forcing u_{00} to also tend to zero. Note that we are not concerned with any singularity, as we focus on M_0^1 with the restriction (4.5). Numerically, this can be seen in Figure 4.

4.4. Asymptotic matching. We now satisfy the asymptotic matching conditions that are required to "glue" the fast and slow dynamics together. By satisfying the matching conditions, we generate the first-order uniform approximation of system (4.1). We additionally show that for a given initial condition, only one of the cases discussed in section 4.3 can satisfy the matching conditions. To obtain a first-order uniform approximation, the following asymptotic matching conditions must be satisfied [20]:

$$\lim_{t_1\to\infty} U_{00}(t_1) = \lim_{t_2\to 0} u_{00}(t_2) = u_m, \tag{4.17a}$$

$$\lim_{t_1\to\infty} V_{00}(t_1) = \lim_{t_2\to 0} v_{00}(t_2) = v_m, \tag{4.17b}$$

$$\lim_{t_1\to\infty} W_{00}(t_1) = \lim_{t_2\to 0} w_{00}(t_2) = w_m. \tag{4.17c}$$

The uniform approximations are then given by

$$u_{00}^{(u)}(t_2) = U_{00}(t_2/\delta) + u_{00}(t_2) - u_m, \tag{4.18a}$$

$$v_{00}^{(u)}(t_2) = V_{00}(t_2/\delta) + v_{00}(t_2) - v_m, \tag{4.18b}$$

$$w_{00}^{(u)}(t_2) = W_{00}(t_2/\delta) + w_{00}(t_2) - u_m. \tag{4.18c}$$

In section 4.2 we show that $\lim_{t_1\to\infty} V_{00}(t_1) = \min\{1, \frac{w(0)}{\sigma u(0)}\}$. Also, since U_{00} and V_{00} are constant, $\lim_{t_1\to\infty} U_{00}(t_1) = u(0)$ and $\lim_{t_1\to\infty} W_{00}(t_1) = w(0)$. Thus, in order to satisfy the matching conditions (4.17), we require $\lim_{t_2\to 0} u_{00}(t_2) = u(0) = u_m$, $\lim_{t_2\to 0} w_{00}(t_2) = w(0) = w_m$, and $\lim_{t_2\to 0} v_{00}(t_2) = \min\{1, \frac{w(0)}{\sigma u(0)}\} = v_m$. It is clear that conditions (4.17a) and (4.17c) can be easily satisfied by adjusting the initial conditions of the slow system.

Now, if $\frac{w(0)}{\sigma u(0)} > 1$, then $v_m = 1$. This means that as t_2 tends to zero, v_{00} must tend to one. Hence, for small t_2, the dynamics must be restricted to M_0^0. However, eventually condition (4.4) will be violated. We address this issue in the next section. Alternatively, if $\frac{w(0)}{\sigma u(0)} \le 1$, then $v_m = \frac{w(0)}{\sigma u(0)}$. Thus, for small t_2, the dynamics must be restricted to M_0^1 to avoid violating (4.4). Unfortunately, the solution for u_{00} can only be given implicitly. However, we can still apply the matching conditions to obtain the first-order approximation numerically.

4.5. The "switch" from M_0^0 to M_0^1. In this section we address the issue that if the slow system dynamics are restricted to M_0^0, then eventually the condition (4.4) is violated. To maintain the inequality (4.4), we allow the dynamics to switch from M_0^0 to M_0^1 at some point in time. The dynamics are shown in Figure 5.

We assume that $\frac{w(0)}{\sigma u(0)} > 1$; then the solution to system (4.11) is restricted to M_0^0 to match with the inner solution. However, it is clear that u_{00} will tend to the stable positive equilibrium, resulting in w_{00} decreasing and eventually violating condition (4.4). Since w_{00} is decreasing to zero, v_{00} is held constant at one, and u_{00} tends toward a positive equilibrium, there must exist a time, t_s, when $w_{00} = \sigma u_{00} v_{00}$. If the slow dynamics, governed by system (4.11), remain on M_0^0 for $t > t_s$, then condition (4.4) is violated for all $t > t_s$.

However, at time t_s, $w_{00} = \sigma u_{00} v_{00}$, and this point is on the curve $\mathcal{C} = M_0^0 \cup M_0^1$. Thus, to ensure that the biological conditions remain satisfied for all time, we require the slow system to undergo a switch. In other words, the dynamics of the slow timescale are governed by system (4.11) restricted to M_0^0 for time $t \le t_s$ and restricted to M_0^1 for time $t > t_s$. For $t > t_s$, v_{00} is no longer restricted to be equal to one, and the equilibrium equation for u_{00} changes. If $\frac{w(0)}{\sigma u(0)} \le 1$, then the slow dynamics are restricted to M_0^1, and no conditions will be violated; hence, no switch is necessary.

The approximation is now able to capture the sudden decrease found in the dynamics. We explain this biologically as a switch that occurs. The switch happens once the nutrient uptake is limited by the cell quota or by the available nutrient. The case in section 4.3.1 assumes that the available nutrient is ample; thus, the cell quota will be high. The case in section 4.3.2 assumes that the available nutrient is limited; thus, the cell quota and CB biomass will be low.

When allowing the switch, we are able to define u_{00}, v_{00}, and w_{00} such that no biological restrictions are broken. If the slow dynamics are restricted to M_0^0 for $t_2 \le t_s$ and restricted to M_0^1 for $t_2 > t_s$, then (4.4) is not breached, and we are able to form

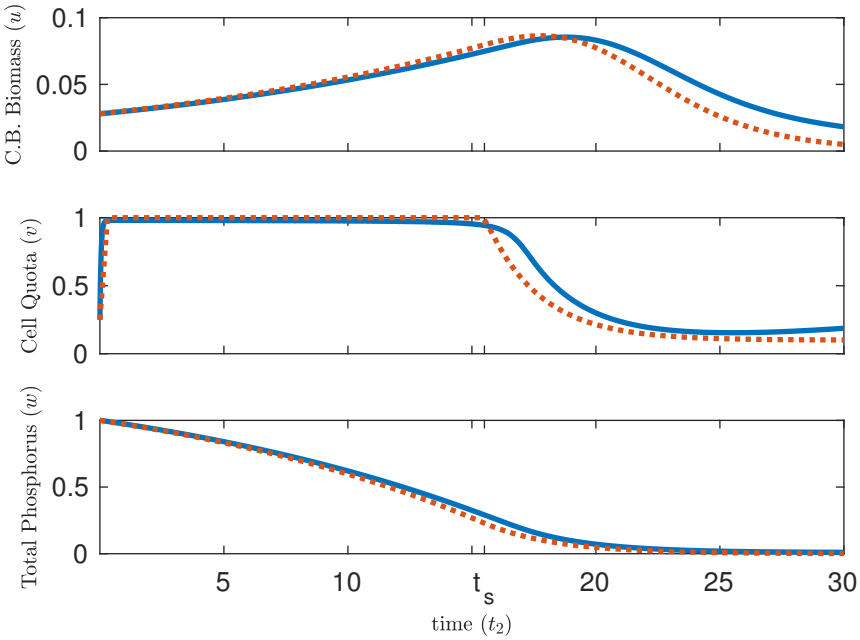

FIG. 5. *Dynamics of the uniform approximation and simulation of the full system for initial conditions such that* $\frac{w(0)}{\sigma u} > 1$. *The dotted line shows the first-order uniform approximation of system* (4.1) *given by* (4.18). *Recall that the dynamics undergo a "switch" at time* t_s. *The solid line shows the dynamics of the full system* (4.1).

the uniform approximation discussed in section 4.4. Figure 5 shows the first-order approximation compared to the numerical solution.

If the initial conditions are such that $w(0)/\sigma u(0) \leq 1$, then by restricting the dynamics to M_0^0 on the slow timescale, we cannot satisfy the matching conditions. Hence, the slow dynamics are governed by (4.16), and the system does not switch. Figure 6 shows the approximation in this case.

5. Geometry of the critical manifold. In this section we combine the above sections to understand analytically and visually the mechanisms that drive the dynamics discussed in Figure 1. We show that the "switch" discussed in section 4.5 is motivated by a loss of hyperbolicity of M_0^0 and M_0^1, both of which are subsets of the critical manifold M_0. Biologically, this is related to the gradual depletion of available phosphorus. Recall that the system (4.1) is defined on the domain $\mathcal{D} = \{(u, v, w) | u, w \geq 0, w - \sigma uv \geq 0, \frac{1}{\gamma} \leq v \leq 1\}$ and that functions g, f and h are defined in (4.1a), (4.1b), and (4.1c), respectively.

5.1. Characteristics of the submanifolds. Here, we look at the reduced system given by (4.11). The variables u, v, w are confined by the equation $(1 - v)\frac{w - \sigma uv}{w - \sigma uv + \mu} = 0$ as they flow on the slow timescale. We show the hyperbolicity criterion of the two sets M_0^0 and M_0^1. The critical manifold, M_0, is contained in the set $f(u, v, w; 0) = 0$.

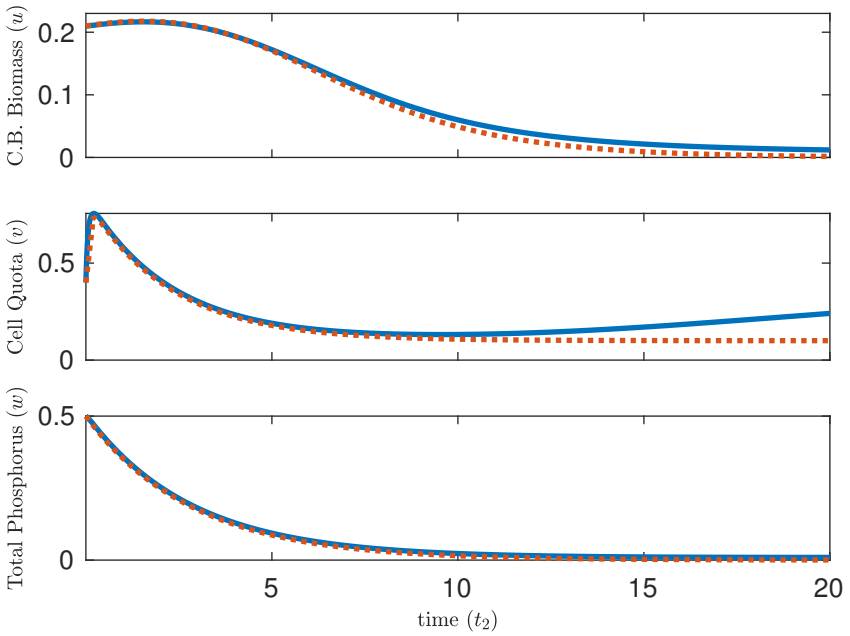

FIG. 6. *Dynamics of the first-order uniform approximation and simulation of the full system for initial conditions such that* $\frac{w(0)}{\sigma u} \leq 1$. *The dotted line shows the first-order uniform approximation of system* (4.1) *given by* (4.18). *Recall that the dynamics do not undergo a "switch" in this case. The solid line shows the dynamics of the full system* (4.1).

5.1.1. Hyperbolicity of M_0^0. To determine the hyperbolicity of M_0^0 in the system's domain, we examine the eigenvalues of

$$\frac{\partial f}{\partial v}(u,v,w;0)|_{M_0^0} = \frac{\partial}{\partial v}(1-v)\frac{w-\sigma uv}{w-\sigma uv+\mu}\Big|_{M_0^0} \tag{5.1}$$

$$= \frac{(\sigma u - w)}{(w-\sigma u+\mu)}. \tag{5.2}$$

It is convenient that the manifold M_0^0 is normally hyperbolic in the entire domain, except along the curve described by $\mathcal{C}$. Furthermore, we notice that the eigenvalues of $\frac{\partial f}{\partial v}(u,v,w;0)|_{M_0^0 \cap \mathcal{D}}$ have negative real parts everywhere except on the curve $\mathcal{C}$. This implies that M_0^0 has a three-dimensional stable manifold $W^s(M_0^0)$ [10] and a two-dimensional unstable manifold $W^u(M_0^0)$ that we conjecture to be M_0^0 itself given the dynamics of the fast system.

5.1.2. Hyperbolicity of M_0^1. Likewise, we examine the hyperbolicity of the submanifold M_0^1 on $\mathcal{D}$ by determining the eigenvalues of $\frac{\partial f}{\partial v}(u,v,w;0)|_{M_0^1}$. From previous calculations,

$$\frac{\partial f}{\partial v}(u,v,w;0)|_{M_0^1} = \frac{\partial}{\partial v}(1-v)\frac{w-\sigma uv}{w-\sigma uv+\mu}\Big|_{M_0^1} \tag{5.3}$$

$$= \frac{(\sigma uv - w)(w-\sigma uv+\mu)+\sigma\mu u(v-1)}{(w-\sigma uv+\mu)^2}\Big|_{M_0^1}$$

$$= \frac{\sigma\mu u(v-1)}{\mu^2}. \tag{5.4}$$

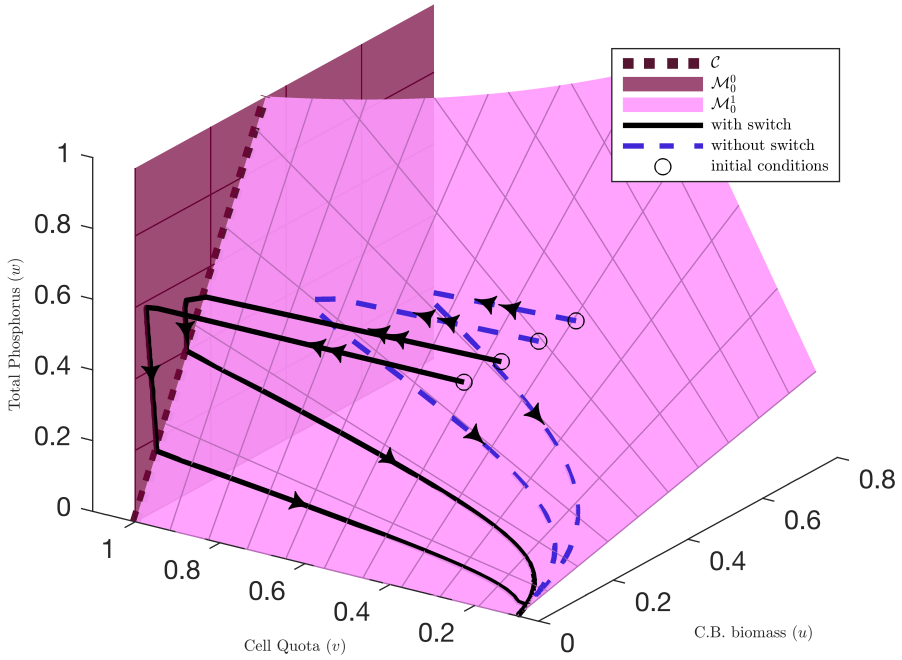

FIG. 7. *Geometric orientation of M_0^0 in burgundy and M_0^1 in pink. Trajectories for various initial conditions are shown. Trajectories with initial conditions such that $\frac{w(0)}{\sigma u(0)} > 1$ are in black and in blue (dashed) otherwise. All trajectories start away from M_0^0 and M_0^1. The double arrow indicates the fast dynamics (away from M_0^0 and M_0^1) and the single arrow the slow dynamics (on or near M_0^0 or M_0^1). The curve $\mathcal{C}$ indicated in dark red (dotted) is the curve where hyperbolicity is lost on each manifold. When the trajectories approach $\mathcal{C}$, the dynamics switch from M_0^0 to M_0^1 as discussed in section* 4.5.

Thus, it is clear that the manifold M_0^1 is hyperbolic on the set defined by $\mathcal{D}\backslash(\{v = 1\} \cup \{u = 0\})$. Again the eigenvalues have negative real parts where M_0^1 is hyperbolic, implying that M_0^1 has a three-dimensional stable manifold $W^s(M_0^1)$ and a two-dimensional unstable manifold $W^u(M_0^1)$ [10] that we conjecture to be M_0^1 itself.

Figure 7 shows the visual representation of the manifolds and corresponding dynamics. First, we note that the dynamics initially tend toward M_0^0. This is the fast timescale dynamics discussed in section 4.2. If the initial conditions are such that no switch needs to occur, the fast dynamics are "cut off" by M_0^1 and approach M_0^1 instead. Finally, we can see that the dynamics on M_0^0 transition to M_0^1 as it approaches the curve $\mathcal{C}$. This figure illustrates where the "switch" occurs geometrically and the role of the fast timescale.

6. Approximation of the switching time. Here, we reexamine the slow system (4.1). In particular we study the dynamics restricted to M_0^0 to better study the switching time, t_s. That is, we are interested in approximating the time it takes for the dynamics to intersect the curve $\mathcal{C}$. We can numerically compute t_s from the numerical solutions of system (4.15). Unfortunately, it is impossible to write t_s as an explicit function of model parameters without making certain approximations.

By graphical inspection, we observe that the function $ug(u, 1; 0)$ resembles a quadratic polynomial. In the region we are concerned with, $v_{00} = 1$. Hence, we can

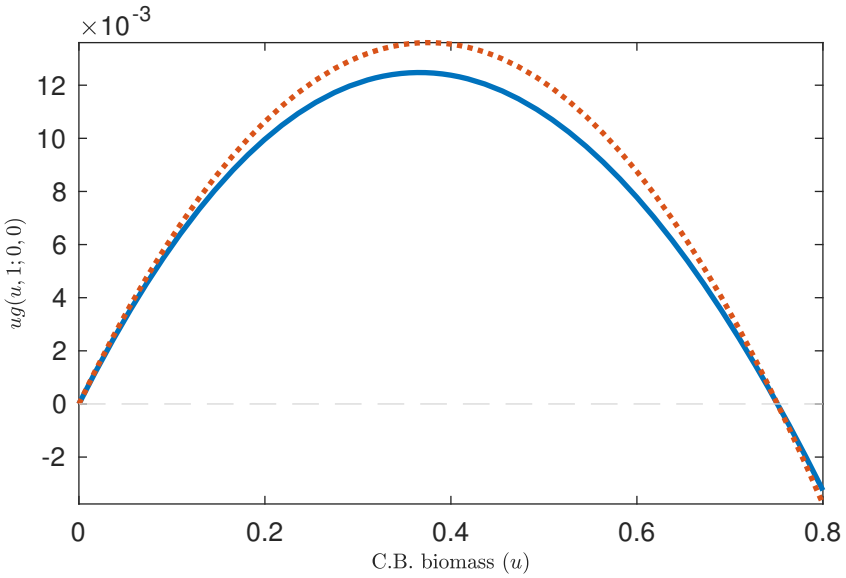

FIG. 8. *Comparison of the curves* $ug(u,1;0)$ *(dotted line) and its approximation* $au(u-u^*)$ *(solid line) given by* (6.1).

postulate that the approximation is of the form au^2+bu+c. We further know that $u=0$ satisfies $ug(u,1,0)=0$ [37]. Hence, in our approximation, $c=0$. Furthermore, as shown by Wang et al. [37], $g(u,1,0)=0$ has a positive unique solution. Thus, we can rewrite the approximation in the form

$$ug(u,1;0,0)\approx au(u^*-u), \tag{6.1}$$

where u^* is the mentioned positive solution, which also represents the biomass during a bloom, and a is to be determined. We determine a by equating the derivatives at $u=0$. In other words, $au(u^*-u)'|_{u=0}=((ug)'|_{u=0}$. Then we obtain

$$a=\left[\left(1-\frac{1}{\gamma}\right)\frac{1}{k_1}\log\left(\frac{1+I}{1+I\exp(-k_1)}\right)-\alpha\right]\frac{1}{u^*}.$$

Figure 8 shows the comparison between $ug(u,1;0)$ and the approximation.

Now we can form an approximation of system (4.15) where $v_{00}=1$. We denote with a tilde the approximation of the first-order solution (i.e., $\tilde{u}\approx u_{00}$):

$$\begin{aligned}\frac{d\tilde{u}}{dt_2}&=a\tilde{u}(u^*-\tilde{u}),\\ \frac{d\tilde{w}}{dt_2}&=-\alpha\sigma\tilde{u}.\end{aligned} \tag{6.2}$$

We solve the first differential equation for $\tilde{u}$ as

$$\tilde{u}=\frac{Cu^*e^{au^*t_2}}{1+Ce^{au^*t_2}}, \tag{6.3}$$

where $C=u(0)/(u^*-u(0))$. Then, solving for $\tilde{w}$ from the second differential equation,

we obtain

$$\frac{d\tilde{w}}{dt} = -\alpha\sigma \frac{Cu^* e^{au^* t}}{1 + Ce^{au^* t}}, \tag{6.4}$$

$$\tilde{w} + B = \int -\alpha\sigma \frac{Cu^* e^{au^* t}}{1 + Ce^{au^* t}} dt, \tag{6.5}$$

$$\tilde{w} + B = \frac{-\alpha\sigma}{a} \log(1 + Ce^{au^* t}), \tag{6.6}$$

where $B = \frac{-\alpha\sigma}{a} \log(1 + C) - w(0)$ in order to satisfy initial conditions; t_s is the time that satisfies the equation $\tilde{w} = \sigma\tilde{u}$, or

$$\frac{-\alpha\sigma}{a} \log(1 + Ce^{au^* t}) - B = \sigma \frac{Cu^* e^{au^* t}}{1 + Ce^{au^* t}}. \tag{6.7}$$

Now, recall that $C = \frac{u(0)}{u^* - u(0)}$. Hence, if our initial condition for CB is such that the ratio between u^* and $u(0)$ is small, which is generally true when the CB biomass does not start in a bloom state, we can approximate $\log(1 + Ce^{u^* at})$ with $Ce^{u^* at}$. Of course, this is only valid if $e^{u^* at}$ does not become large. However, the right-hand side of (6.7) is bounded and positive. The left-hand side of (6.7) is monotone decreasing with respect to t and for large values of t is negative. Hence, the solution of (6.7), if it exists, remains bounded. Thus, the approximation remains valid. We approximate the time t_s by solving (6.7). For simplicity, let $x = Ce^{au^* t}$; then (6.7) becomes

$$\begin{aligned} &\frac{-\alpha\sigma}{a} x - B = \sigma \frac{u^* x}{1 + x} \\ &\iff \quad 0 = x^2 + \Big(1 + B\frac{a}{\alpha\sigma} + \frac{au^*}{\sigma}\Big)x + B\frac{a}{\alpha\sigma}. \end{aligned}$$

It is easily verified that $B\frac{a}{\alpha\sigma} < 0$; thus, following Descartes' rule of sign, there is one positive and one negative solution to the above equation. We are only interested in the positive solution expressed as

$$x_s = -\frac{1}{2}\Big(1 + B\frac{a}{\alpha\sigma} + \frac{au^*}{\sigma}\Big) + \sqrt{\frac{1}{4}\Big(1 + B\frac{a}{\alpha\sigma} + \frac{au^*}{\sigma}\Big)^2 - B\frac{a}{\alpha\sigma}} > 0.$$

Thus,

$$t_s = \log(x_s/C)/au^*. \tag{6.8}$$

Figure 9 shows the value of t_s as a function of the initial condition for w. In this situation, $w(0)$ is easily related to the level of eutrophication. We further note that t_s is nonnegative for reasonable values of $w(0)$, mainly those satisfying condition (4.4). Furthermore, the values of t_s computed are reasonable when compared to real-life HAB times [33, 38].

7. Biological interpretation. We now discuss how the analysis allows us to understand the biological mechanisms on a deeper level. In fact, we extend the results regarding the dynamics on the critical manifold to relate them back to the singularly perturbed system (4.1) with $\beta = 0$. In doing this, we show that the flow of our singularly perturbed system, restricted to the slow manifold, is a small perturbation of the dynamics covered in the subsystem analysis. Also, the stable and unstable manifolds

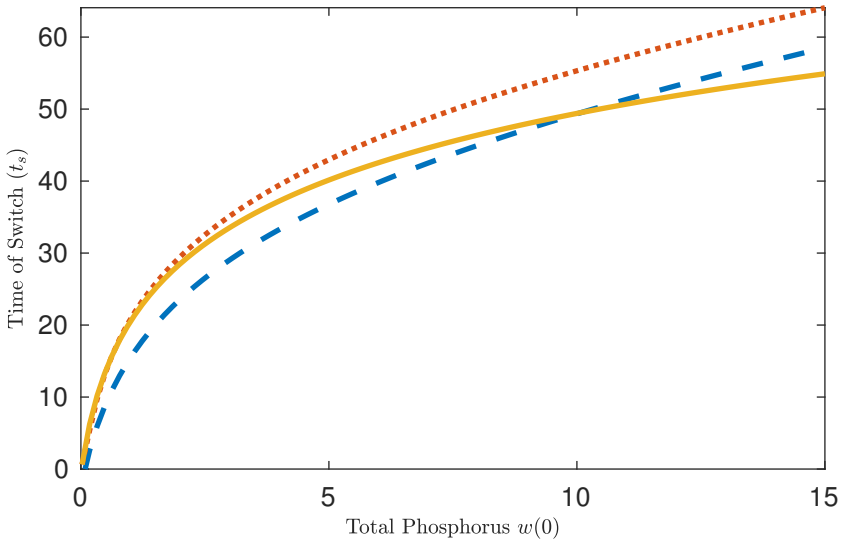

FIG. 9. *Switching time t_s as a function of $w(0)$. The initial condition $w(0)$ serves as a proxy for initial level of eutrophication. The solid curve gives t_s computed using the approximation given in* (6.8). *The dashed and dotted curves give t_s as the implicit solution of* (6.7) *and numerical value from simulations of system* (4.1) *for given values of $w(0)$, respectively.*

of the reduced system and the full system can be related by a small perturbation. We refer the reader to Appendix B.1 for the details. As discussed in Appendix B.1, we conclude that the biological interpretation of the reduced system is also applicable to the full system.

First, we assume $\frac{w(0)}{\sigma u(0)} > 1$, which implies that phosphorus is not limiting. The fast system (4.3) has V_{00} approaching 1. To satisfy the matching conditions, we require the slow dynamics to be restricted to M_0^0 initially. M_0^0 is described as the surface where cell quota is maximal, which is biologically consistent with the assumption of sufficient phosphorus. Now, the slow scale dynamics are governed by (4.11) restricted to M_0^0. We have shown that u_{00} approaches a positive equilibrium while w_{00} decreases. Biologically, since there is sufficient phosphorus, it is clear that CB will grow until growth is limited by light. Also, we expect the total phosphorus to decline as it is being exchanged. Eventually, at time t_s, w_{00} will have decreased such that $w_{00} = \sigma u_{00} v_{00}$. This is also the point in time where the flow on M_0^0 intersects M_0^1. Biologically, we describe this as the point where phosphorus becomes limiting. At t_s, the slow dynamics switch and are now governed by (4.11) restricted to M_0^1. We describe manifold M_0^1 as being phosphorus limited; thus, we expect and observe CB collapse. Figure 7 shows these dynamics with respect to the manifolds. Figure 5 shows these dynamics with respect to time. In other words, Figure 5 shows the complete uniform approximation and its relation to the dynamics of the full system (4.1).

Now, if $\frac{w(0)}{\sigma u(0)} < 1$, the dynamics are simpler. This initial condition implies, biologically, that phosphorus will be limited. On the fast timescale, we see V_{00} approach $\frac{w(0)}{\sigma u(0)}$, which is less than the maximal cell quota. This implies that nutrient is limiting. However CB can still grow, depending on the nutrient limitation compared to the initial condition. To satisfy the matching condition, the slow dynamics are restricted to M_0^1, the limited nutrient manifold. There is no switch on the slow timescale, and

the CB simply decline along with the total phosphorus. Figure 7 shows this dynamic with respect to the manifolds, and Figure 6 compares the uniform approximation to the full system (4.1).

The details in Appendix B.1 allow us to draw the conclusion that the dynamics of the reduced system are a small perturbation of the dynamics of the full system with $\beta = 0$. Hence, we conclude that the biological interpretation of the reduced system dynamics, described above, is also valid for the dynamics of the full system. Furthermore, we are able to interpret the geometry of the system biologically, leading to a deeper knowledge of CB systems.

8. Discussion. CB are incredibly common in freshwater ecosystems. In fact, it is rare to encounter a freshwater environment where CB are absent. The prevalence of CB often has a negative impact on water treatment costs, recreation, and aquatic health. The potential socioeconomic impact of CB motivates the complete understanding of their dynamics, in particular their short-term dynamics. Several papers have successfully gained further insight into algae and CB dynamics [24, 37, 15, 2, 4], but there is still much more that can be understood. In this paper we attempt to understand the transient CB dynamics for various eutrophic initial states.

We study the previously established and well-studied stoichiometric models of Wang et al. [37] and Berger et al. [2]. The mechanistic structure of the model, as well as the dynamics, lead to a multiple timescale analysis. We find that δ is a small parameter that acts as a singular perturbation. This is not surprising, as δ is proportional to the difference between the maximum and minimum cell quota. The cell quota, Q, measures the phosphorus-to-carbon ratio inside of a single cell. This ratio is naturally small for almost all living organisms but varies significantly for CB [38]. The other two variables, B and R, measure concentrations of CB carbon biomass and total phosphorus respectively, which are large compared to the phosphorus-to-carbon ratio of a single cell. Due to the difference of magnitude between our state variables, it is intuitive that the system yields a multiscale dynamic. Also, we observe in Figure 1 abrupt transition layers that were not fully understood. For these reasons, an analysis of multiple timescales is performed.

We have shown that the fast system behaves as follows: Both the CB biomass and the dissolved phosphorus concentrations are constant, and the cell quota will increase monotonically toward $\min\{1, \frac{w(0)}{\sigma u(0)}\}$. This implies that the P uptake occurs on the fast timescale, whereas CB growth and nutrient depletion are slower processes.

The slow scale analysis yields an interesting structure of the critical manifolds for system (4.11). The critical manifold can be broken down into two submanifolds, M_0^0 and M_0^1. We interpret M_0^0 as representing the dynamics when nutrient is sufficient; alternatively, M_0^1 describes the dynamics when nutrient is insufficient. The two submanifolds are hyperbolic everywhere except near their intersection, which is denoted as the curve $\mathcal{C}$. If the initial condition has sufficient nutrient, the dynamics will quickly approach M_0^0. On the other hand, when the initial condition has insufficient available phosphorus, the dynamics quickly approach M_0^1. When nutrient is sufficient, the cell quota is maximal, the CB biomass is high, and the CB can grow until phosphorus is depleted or when the dynamics leave M_0^0 by approaching $\mathcal{C}$. When the dynamics, initially with sufficient nutrient, approach $\mathcal{C}$, an abrupt transition must occur to avoid biological violations. This transition is described as a switch in the dynamics from sufficient nutrient to insufficient. This switch is analogous to jump points, or fold points described in the literature [20, 10]. On M_0^1, available phosphorus is insufficient

to support a high CB biomass, forcing a crash of the bloom. This insight is consistent with what is believed to drive CB dynamics. That is, it is commonly believed that a more eutrophic state will yield larger CB biomass. Furthermore, light is also crucial in bloom formation but often not the limiting resource [28, 38, 25]. Biologically, the concept of "sufficient" nutrient for a population has not yet been adequately described. This work can help suggest what "sufficient" nutrient means from a mathematical perspective.

Furthermore, the analysis described in sections 4 and 5 makes it possible to compute an approximation for the biologically relevant switching time discussed in section 6. We describe the switching time, t_s, approximated by (6.8), as the time it takes for the flow to transition from the sufficient phosphorus manifold (M_0^0) to the insufficient phosphorus manifold (M_0^1). Given the interpretation of the submanifolds, the computation of t_s allows us to approximate the longevity of a bloom with respect to reasonable model parameter values. In particular, t_s depends on the initial condition for total phosphorus (Figure 9), which serves as a proxy for the eutrophic state. Our approximation of bloom longevity is of similar scale to what is observed in real aquatic ecosystems [33].

Finally, we applied the classical results of Neil Fenichel to relate the dynamics of the reduced system (4.11) to the dynamics of the full model (4.1) (see Appendix B.1) [10, 7]. The reduced system allows us to provide a meaningful biological interpretation of the driving mechanisms, and Fenichel's theorems show that the interpretation is applicable to the full system.

Our model assumes that the input nutrient from the hypolimnion, rivers, and runoff is constant. Realistically, the concentrations of inputs are varying, and large amounts of phosphorus are suddenly added after rainfall events or spring runoff [28, 33]. Interestingly, our model can easily be extended to account for impulsively added phosphorus. Figure 10 shows the three-year dynamics when considering large but varying annual inputs of phosphorus. The impulsive model can make for a more realistic long-term understanding of the dynamics with respect to the within-year transient dynamics. Also, it has been shown that for large values of z_m, CB will not persist [37]. This illustrates the importance of epilimnion depth in CB dynamics; however, we do not consider variations of z_m in this analysis. While our model assumes a stratified lake, many temperate lakes are dimictic or polymictic, meaning stratification is broken occasionally throughout the year [16], causing complex changes in the CB density and nutrient distribution [5]. The factors listed above are important to CB dynamics and should be considered in future work. Although slight changes of our results will occur upon consideration of these factors, we expect that the main driving mechanisms shown here are robust. That is, additional mechanisms will enhance the reality of our model but would still likely act as perturbations of the reduced models (4.3) and (4.11), in which the driving mechanisms were established.

Our analysis has shed light on the mechanisms driving certain aspects of CB dynamics. However, certain aspects are still left to be mathematically explained, namely, the nonzero low CB biomass phase seen in Figure 1. Our analysis suggests that the CB biomass will tend to zero, which is not true of the full model and generally not true biologically. We suspect that considering the perturbation parameter, β, to be nonzero will allow us to understand this phase of the dynamics. However, analysis of the higher-order approximations is not considered here and should be considered in the future.

CB are considered primary producers; thus, organisms in higher trophic levels depend directly on CB dynamics. This study helps build a framework to study tran-

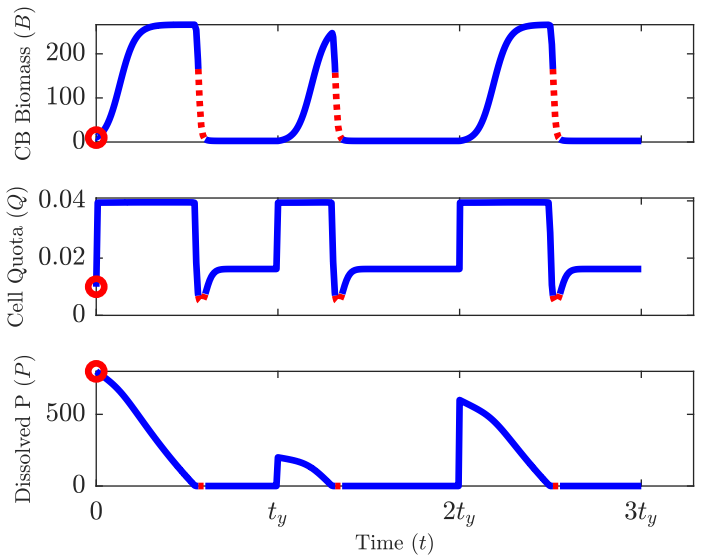

FIG. 10. *Three-year dynamics of system* (2.4) *with varying phosphorus impulses each year* (t_y).

sient aquatic dynamics in eutrophic conditions. Future work could include the study of symbiotic, predator-prey, and competitive interactions that depend on the CB transient dynamics. Furthermore, cyanotoxins are a large global concern that affect agriculture, recreation, water treatment, and aquatic organisms. This model can be extended to consider cyanotoxin production and its influences on aquatic interactions.

To our knowledge, analysis of the form in this paper has not been performed on any stoichiometric model in ecology. These results are important for future work in studying the transient dynamics of CB as well as building a framework to study transient dynamics in other ecological stoichiometry models. Specifically, they are useful in determining the mechanisms that motivate each aspect of the transient dynamics.

Appendix A. Two-parameter asymptotic expansion. For a given function, $f(t)$, we define its two-parameter asymptotic expansion, in *beta* and δ, as follows:

$$f(t) = \sum_{i,j\geq 0} \beta^i \delta^j f_{i,j}(\tau) = f_{0,0} + \beta f_{1,0} + \delta f_{0,1} + \beta\delta f_{1,1} + \cdots . \tag{A.1}$$

Appendix B. Fenichel's theorems. We begin by constructing a general singular perturbed system

$$\frac{du}{dt} = f(u, v; \epsilon), \tag{B.1a}$$

$$\frac{dv}{dt} = \epsilon g(u, v; \epsilon), \tag{B.1b}$$

where ϵ is a small parameter and the variable u is considered the fast variable and v the slow variable. Assume $u \in \mathbf{R}^k$. We denote the critical manifold as $\mathcal{M}_0$, where $\mathcal{M}_0$ is a subset of fixed points of (B.1a), and naturally assume it to be a k-dimensional manifold. The results of Fenichel can be applied to system (B.1).

THEOREM B.1 (Fenichel's first theorem [10]). *Suppose* $\mathcal{M}_0 \subset \{f(u,v;0) = 0\}$ *is compact, possibly with boundary, and normally hyperbolic. Suppose* f *and* g *are smooth. Then for* $\epsilon > 0$ *and sufficiently small, there exists a manifold* $\mathcal{M}_\epsilon$, $\mathcal{O}(\epsilon)$ *close and diffeomorphic to* $\mathcal{M}_0$ *that is locally invariant under the flow of the full problem* (B.1).

THEOREM B.2 (Fenichel's first theorem [10]). *Suppose* $\mathcal{M}_0 \subset \{f(u,v;0) = 0\}$ *is compact, possibly with boundary, and normally hyperbolic. Suppose* f *and* g *are smooth. Then for* $\epsilon > 0$ *and sufficiently small, there exist manifolds* $W^s(\mathcal{M}_\epsilon)$ *and* $W^u(\mathcal{M}_\epsilon)$ *that are* $\mathcal{O}(\epsilon)$ *close and diffeomorphic to* $W^s(\mathcal{M}_0)$ *and* $W^s(\mathcal{M}_0)$, *respectively, and that are locally invariant under the flow of* (B.1)

Note that in the context of system (4.1) the manifolds M_0^0 and M_0^1 are not normally hyperbolic. However, by removing a neighborhood of the curve $\mathcal{C}$,$\mathcal{N}(\mathcal{C};\epsilon)$ from M_0^0 and M_0^1, we create normally hyperbolic manifolds. That is, the manifolds M_0^{0h} and M_0^{1h} defined in section B.1 are normally hyperbolic. Theorems B.3 and B.4 are then direct results of Fenichel's first and second theorems, respectively.

B.1. Fenichel's theorems applied. Here, we apply Fenichel's theorems to show that the flow of our singularly perturbed system, restricted to the slow manifold, is a small perturbation of the dynamics covered in the subsystem analysis. Furthermore, the stable and unstable manifolds of the reduced system and the full system can be related by a small perturbation.

Recall that β acts as a regular perturbation parameter of system (4.1). Since the theory presented in this section is relevant to singular perturbations, we set, for simplicity, $\beta = 0$.

Consider the critical manifold $M_0 \subset M_0^0 \cup M_0^1 = \{f(u,v,w;0,0) = 0\} \cap \mathcal{D}$. We introduce an open epsilon neighborhood of the curve $\mathcal{C}$ by $\mathcal{N}(\mathcal{C};\epsilon) = \{x = (u,v,w) \in \mathcal{D} \mid d(x;\mathcal{C}) < \epsilon\}$, where $0 < \epsilon \ll 1$ and $d(x;A)$ is the least distance from a point x to a set A. We further denote the manifolds $M_0^{0h} = M_0^0 \backslash \mathcal{N}(\mathcal{C};\epsilon)$ and $M_0^{1h} = M_0^1 \backslash \mathcal{N}(\mathcal{C};\epsilon)$. Now, our critical manifold consists of two hyperbolic sets and a small set near the nonhyperbolic set.

We can apply the results of Fenichel to obtain the following results.

THEOREM B.3 (see [10, 7]). *For* $\delta > 0$ *and sufficiently small, there exist manifolds* M_δ^0 *and* M_δ^1, $\mathcal{O}(\delta)$ *that are close and diffeomorphic to* M_0^{0h} *and* M_0^{1h}, *respectively, that are locally invariant under the flow of the system* (4.1) *with* $\beta = 0$.

In essence, Theorem B.3 implies that the flow of system (4.1) with $\beta = 0$, when restricted M_δ^0 or M_δ^1, is an order δ perturbation of the flow of system (4.11) on the respective submanifolds M_0^{0h} or M_0^{1h}. Furthermore, we can say that the dynamics on M_δ will remain on M_δ, except perhaps at the boundary of M_δ. We note that the sets M_δ^0 and M_δ^1 are, in general, not sets of fixed points, and hence stability of these manifolds is thought of in a different manner. The following theorem alludes to the the "stability" of our system.

THEOREM B.4 (see [10, 7]). *For* $\delta > 0$ *and sufficiently small, there exist manifolds* $W^s(M_\delta^0)$ $(W^s(M_\delta^1))$ *and* $W^u(M_\delta^0)$ $(W^u(M_\delta^1))$ *that are* $\mathcal{O}(\delta)$ *close and diffeomorphic to* $W^s(M_0^{0h})$ $(W^s(M_0^{1h}))$ *and* $W^u(M_0^{0h})$ $(W^u(M_0^{1h}))$, *respectively, and that are locally invariant under the flow of the system* (4.1) *with* $\beta = 0$.

Since M_δ^0 and M_δ^1 are not sets of fixed points (unlike M_0^{0h} and M_0^{1h}), we discuss what the notation of stability means with respect to M_δ^0 and M_δ^1. The manifold $W^s(M_\delta^{0,1})$ $(W^u(M_\delta^{0,1}))$ is still referred to as the stable (unstable) manifold. Stability

(or instability) here means that the flow in $W^s(M_\delta^{0,1})$ ($W^u(M_\delta^{0,1})$) decays to $M_\delta^{0,1}$ in forward time (backward time) [20, 10]. The details of the these results are shown in Appendix B.

Theorems and B.3 and B.4 are direct results of Fenichel's first and second theorem, respectively. The details of Fenichel's theorems are covered in Appendix B.

The above theorems allow us to draw the conclusion that the dynamics of the reduced system are a small perturbation of the dynamics of the full system with $\beta = 0$. Hence, we conclude that the biological interpretation of the reduced system dynamics is also valid of the dynamics of the full system.

Acknowledgments. We would like to thank Professor Rolf Vinebrooke for the stimulating biological discussions. In addition, we thank the two reviewers for their helpful comments.

REFERENCES

[1] T. Andersen, J. J. Elser, and D. O. Hessen, *Stoichiometry and population dynamics*, Ecol. Lett., 7 (2004), pp. 884–900, https://doi.org/10.1111/j.1461-0248.2004.00646.x.

[2] S. A. Berger, S. Diehl, T. J. Kunz, D. Albrecht, A. M. Oucible, and S. Ritzer, *Light supply, plankton biomass, and seston stoichiometry in a gradient of lake mixing depths*, Limnol. Oceanogr., 51 (2006), pp. 1898–1905, https://doi.org/10.4319/lo.2006.51.4.1898.

[3] R. Bertram and J. E. Rubin, *Multi-timescale systems and fast-slow analysis*, Math. Biosci., 287 (2017), pp. 105–121.

[4] S. Diehl, S. Berger, and R. Wöhrl, *Flexible nutrient stoichiometry mediates environmental*, Ecology, 86 (2005), pp. 2931–2945, https://esajournals.onlinelibrary.wiley.com/doi/pdf/10.1890/04-1512.

[5] E. J. Griffith, A. Beeton, J. M. Spencer and D. T. Mitchell, *Environmental Phosphorus Handbook*, Wiley, New York, 1973.

[6] J. J. Elser, T. H. Chrzanowski, R. W. Sterner, and K. H. Mills, *Stoichiometric constraints on food-web dynamics: A whole-lake experiment on the Canadian shield*, Ecosystems, 1 (1998), pp. 120–136, https://link.springer.com/content/pdf/10.1007{%}2Fs100219900009.pdf.

[7] N. Fenichel, *Geometric singular perturbation theory ordinary differential equations*, J. Differential Equations, 31 (1979), pp. 53–98, https://doi.org/10.1016/0022-0396(79)90152-9.

[8] J. P. Grover, *The impact of variable stoichiometry on predator-prey interactions: A multi-nutrient approach*, Amer. Nat., 162 (2003), pp. 29–43, https://doi.org/10.1086/376577.

[9] A. Hastings, K. C. Abbott, K. Cuddington, T. Francis, G. Gellner, Y. C. Lai, A. Morozov, S. Petrovskii, K. Scranton, and M. L. Zeeman, *Transient phenomena in ecology*, Science, 361 (2018), https://doi.org/10.1126/science.aat6412.

[10] G. Hek, *Geometric singular perturbation theory in biological practice*, J. Math. Biol., 60 (2010), pp. 347–386, https://doi.org/10.1007/s00285-009-0266-7.

[11] D. O. Hessen, J. J. Elser, R. W. Sterner, and J. Urabe, *Ecological stoichiometry: An elementary approach using basic principles*, Limnol. Oceanogr., 58 (2013), pp. 2219–2236, https://doi.org/10.4319/lo.2013.58.6.2219.

[12] A. L. Hodgkin and A. F. Huxley, *A quantitative description of membrane current and its application to conduction and excitation in nerve*, J. Physiol., 117 (1952), pp. 500–544, https://doi.org/10.1007/BF02459568.

[13] Q. Huang, L. Parshotam, H. Wang, C. Bampfylde, and M. A. Lewis, *A model for the impact of contaminants on fish population dynamics*, J. Theoret. Biol., 334 (2013), pp. 71–79, https://doi.org/10.1016/j.jtbi.2013.05.018.

[14] Q. Huang, H. Wang, and M. A. Lewis, *The impact of environmental toxins on predator-prey dynamics*, J. Theoret. Biol., 378 (2015), pp. 12–30, https://doi.org/10.1016/j.jtbi.2015.04.019.

[15] J. Huisman and F. J. Weissing, *Light limited growth and competition for light in well mixed aquatic environments: An elementary model*, Ecology, 75 (1994), pp. 507–520, https://doi.org/10.2307/1939554.

[16] J. Kalff, *Limnology: Inland Water Ecosystems*, no. 504.45 KAL, Prentice Hall, Upper Saddle River, NJ, 2002, https://search.library.ualberta.ca/catalog/2595736papers://aff512a5-579d-44ca-9504-d5ff894b570f/Paper/p4515.

[17] J. P. Keener and J. Sneyd, *Mathematical Physiology*, Vol. 8, Springer, New York, 1998, https://doi.org/10.1007/b98841.
[18] J. T. Kirk, *Light and Photosynthesis in Aquatic Ecosystems*, 3rd ed., Cambridge University Press, Cambridge, 2010, https://doi.org/10.1017/CBO9781139168212.
[19] J. D. Kong, P. Salceanu, and H. Wang, *A stoichiometric organic matter decomposition model in a chemostat culture*, J. Math. Biol., 76 (2017), pp. 1–36, https://doi.org/10.1007/s00285-017-1152-3.
[20] C. Kuehn, *Multiple Time Scale Dynamics*, Vol. 191, Springer, New York, 2015, https://doi.org/10.1007/978-3-319-12316-5.
[21] M. Lang, P. Li, and X. Yan, *Runoff concentration and load of nitrogen and phosphorus from a residential area in an intensive agricultural watershed*, Sci. Total Environ., 458–460 (2013), pp. 238–245, https://doi.org/10.1016/j.scitotenv.2013.04.044.
[22] I. Loladze, Y. Kuang, and J. J. Elser, *Stoichiometry in producer-grazer systems: Linking energy flow with element cycling*, Bull. Math. Biol., 62 (2000), pp. 1137–1162, https://doi.org/10.1006/bulm.2000.0201.
[23] C. Martínez, F. Mairet, and O. Bernard, *Theory of turbid microalgae cultures*, J. Theoret. Biol., 456 (2018), pp. 190–200, https://doi.org/10.1016/j.jtbi.2018.07.016.
[24] C. M. Melina Celeste, R. Lorena, A. Jorge Oswaldo, G. Sandro, S. Daniela, A. Dario, and G. Leda, *Mathematical modeling of Microcystis aeruginosa growth and* [*D-Leu* 1] *microcystin-LR production in culture media at different temperatures*, Harmful Algae, 67 (2017), pp. 13–25, https://doi.org/10.1016/j.hal.2017.05.006.
[25] S. Merel, W. David, R. Chicana, S. Snyder, E. Baurès, and O. Thomas, *State of knowledge and concerns on cyanobacterial blooms*, Environ. Int., 59 (2013), pp. 303–327, https://doi.org/10.1016/j.envint.2013.06.013.
[26] F. M. Morel, *Kinetics of nutrient uptake and growth in phytoplankton*, J. Phycol., 23 (1987), pp. 137–150, https://doi.org/10.1111/j.1529-8817.1987.tb04436.x.
[27] H. W. Paerl, *Mitigating harmful cyanobacterial blooms in a human- and climatically-impacted world*, Life, 4 (2014), pp. 988–1012, https://doi.org/10.3390/life4040988.
[28] H. W. Paerl and T. G. Otten, *Harmful cyanobacterial blooms: Causes, consequences, and controls*, Microb. Ecol., 65 (2013), pp. 995–1010, https://doi.org/10.1007/s00248-012-0159-y.
[29] A. Peace, M. D. Poteat, and H. Wang, *Somatic growth dilution of a toxicant in a predator-prey model under stoichiometric constraints*, J. Theoret. Biol., 407 (2016), https://doi.org/10.1016/j.jtbi.2016.07.036.
[30] S. Rinaldi and S. Muratori, *Slow-fast limit cycles in predator-prey models*, Ecol. Model., 61 (1992), pp. 287–308, https://doi.org/10.1016/0304-3800(92)90023-8.
[31] J. Rubin and M. Wechselberger, *Giant squid-hidden canard: The 3D geometry of the Hodgkin-Huxley model*, Biol. Cybernet., 97 (2007), pp. 5–32, https://doi.org/10.1007/s00422-007-0153-5.
[32] R. Sterner and J. Elser, *Ecological Stoichiometry: The Biology of Elements from Molecules to the Biosphere*, Princeton University Press, Princeton, NJ, 2002, https://press.princeton.edu/titles/7434.html.
[33] Z. E. Taranu, R. W. Zurawell, F. Pick, and I. Gregory-Eaves, *Predicting cyanobacterial dynamics in the face of global change: The importance of scale and environmental context*, Glob. Change Biol., 18 (2012), pp. 3477–3490, https://doi.org/10.1111/gcb.12015.
[34] D. B. Van De Waal, J. M. Verspagen, M. Lürling, E. Van Donk, P. M. Visser, and J. Huisman, *The ecological stoichiometry of toxins produced by harmful cyanobacteria: An experimental test of the carbon-nutrient balance hypothesis*, Ecol. Lett., 12 (2009), pp. 1326–1335, https://doi.org/10.1111/j.1461-0248.2009.01383.x.
[35] B. van der Pol, *LXXXVIII. On "relaxation-oscillations,"* London, Edinburgh, Dublin Philos. Mag. J. Sci., 2 (1926), pp. 978–992, https://doi.org/10.1080/14786442608564127.
[36] H. Wang, Y. Kuang, and I. Loladze, *Dynamics of a mechanistically derived stoichiometric producer-grazer model*, J. Biol. Dyn., 2 (2008), pp. 286–296, https://doi.org/10.1080/17513750701769881.
[37] H. Wang, H. Smith, Y. Kuang, and J. J. Elser, *Dynamics of stoichiometric bacteria-algae interactions in the epilimnion*, SIAM J. Appl. Math., 68 (2007), pp. 503–522.
[38] B. A. Whitton, *Ecology of Cyanobacteria* II: *Their Diversity in Space and Time*, Springer, New York, 2012, https://doi.org/10.1007/978-94-007-3855-3.
[39] K. Yoshiyama, J. P. Mellard, E. Litchman, and C. A. Klausmeier, *Phytoplankton competition for nutrients and light in a stratified water column*, Amer. Nat., 174 (2009), pp. 190–203, https://doi.org/10.1086/600113.